



HAL
open science

Experimental validation of an 2D overland flow model using high resolution water depth and velocity data

Luis Cea, Cédric Legout, Frédéric Darboux, Michel Esteves, Guillaume Nord

► To cite this version:

Luis Cea, Cédric Legout, Frédéric Darboux, Michel Esteves, Guillaume Nord. Experimental validation of an 2D overland flow model using high resolution water depth and velocity data. *Journal of Hydrology*, 2014, 513, pp.142-153. 10.1016/j.jhydrol.2014.03.052 . hal-01023524

HAL Id: hal-01023524

<https://hal.science/hal-01023524>

Submitted on 28 May 2020

HAL is a multi-disciplinary open access archive for the deposit and dissemination of scientific research documents, whether they are published or not. The documents may come from teaching and research institutions in France or abroad, or from public or private research centers.

L'archive ouverte pluridisciplinaire **HAL**, est destinée au dépôt et à la diffusion de documents scientifiques de niveau recherche, publiés ou non, émanant des établissements d'enseignement et de recherche français ou étrangers, des laboratoires publics ou privés.

characteristics of the terrain in order to correctly reproduce the flow hydrodynamics.

5 *Key words:* overland flow, 2D shallow water equations, bed roughness, Large
6 Scale Particle Image Velocimetry, laser scanner

7 **1. INTRODUCTION**

8 Several studies on the experimental validation of overland flow models based
9 on the two-dimensional shallow water equations have shown that, with a proper
10 bed friction calibration and a well defined Digital Terrain Model (DTM), these
11 kind of models are able to produce accurate predictions of the outlet hydrograph
12 in a basin (Cea et al., 2010a,b; Howes et al., 2006; Kivva and Zheleznyak, 2005;
13 Morgali and Linsley, 1965; Yan and Kahawita, 1989; Zhang and Cundy, 1989).
14 The evaluation of model performance in all these studies is based on the correct
15 prediction of the outlet hydrograph generated by a rainfall event, which is of most
16 importance for flood forecasting applications. However, a distributed model gives
17 much more information regarding the spatial distribution of water depth and ve-
18 locity, which might be used in contaminant transport and erosion models. In fact,
19 there has been a trend in the last years to develop physically-based water ero-
20 sion and solute transport models including the representation of processes at their
21 lowest scales (Hairsine and Rose, 1992b,a; Jomaa et al., 2010; Nord and Esteves,
22 2007, 2010; Shaw et al., 2006, 2009). These models use formulations that require
23 a very detailed spatial characterization of the flow field (water depth, velocity and
24 bed friction) in order to take advantage of their full potential. The problem of
25 predicting flow transport capacity demands not only a proper sediment transport
26 equation, but a reliable means of modelling overland flow hydraulics on rough

27 surfaces (Abrahams et al., 1998). In this vein, several studies have been devoted
28 to the physical characterization of bed roughness in order to improve the predic-
29 tion capability of overland flow models (Jarvela, 2002; Shaw et al., 2009), and it
30 has been recognized in previous laboratory studies involving overland flow condi-
31 tions that the effective bed roughness coefficient varies substantially with the flow
32 properties due to additional head losses generated by small scale flow features
33 which are not resolved in the numerical models (Fraga et al., 2013; Howes et al.,
34 2006; Lawrence, 2000; Shaw et al., 2006; Tatard et al., 2008).

35 However, an accurate prediction of the outlet hydrograph does not guarantee
36 that the hydraulics within the plot is properly computed, and so such an approach
37 is not a thorough model validation. One of the main conclusions of the work of
38 Tatard et al. (2008) was that the Froude number was not predicted by any of the
39 three models tested on a 40 m² plot and even the general pattern was missed.
40 This highlights the need to evaluate the performance of two-dimensional overland
41 flow models in terms of their capability to reproduce the spatial distribution of
42 water depth and velocity at the same time. Until now, very few studies have made
43 such evaluation. Tatard et al. (2008) compared measured and modelled depths
44 and velocities at selected points without performing a comparison on the whole
45 plot. More recently, Mügler et al. (2011) intended to make an evaluation of what
46 occurs within the plot by comparing measured and modelled tracer breakthrough
47 curves of point-source injection of tracer under rainfall conditions. Such an ap-
48 proach aims at assessing if the actual travel time of a tracer is well reproduced by
49 the model. However, it is a spatially integrated approach that does not allow the
50 direct comparison of observed and modelled depth-velocity maps at the mesh size
51 scale. To the best of our knowledge, the work presented in this paper provides

52 for the first time a direct comparison of modelled and measured water depth and
 53 velocity fields under surface runoff conditions. We present the experimental vali-
 54 dation of a distributed overland flow model based on the two-dimensional shallow
 55 water equations using Large Scale Particle Image Velocimetry (LSPIV) data for
 56 the surface velocity and laser scanner data for the water depth. Six test cases over
 57 two impervious surfaces with different micro and macro-roughness characteristics
 58 are used to validate the model, and to analyze the sensitivity of model performance
 59 to the bed friction parameterization and to the spatial resolution of the DTM and
 60 numerical mesh. In all the test cases the water depth was always less than 10 mm.

61 2. NUMERICAL MODEL AND SOLVER

62 Overland flow models based on the two-dimensional shallow water equations
 63 solve the following depth-averaged mass and momentum conservation equations:

$$\frac{\partial h}{\partial t} + \frac{\partial q_x}{\partial x} + \frac{\partial q_y}{\partial y} = 0 \quad (1)$$

$$\frac{\partial q_x}{\partial t} + \frac{\partial}{\partial x} \left(\frac{q_x^2}{h} + \frac{gh^2}{2} \right) + \frac{\partial}{\partial y} \left(\frac{q_x q_y}{h} \right) = -gh \frac{\partial z_b}{\partial x} - \frac{\tau_{b,x}}{\rho} \quad (2)$$

$$\frac{\partial q_y}{\partial t} + \frac{\partial}{\partial x} \left(\frac{q_x q_y}{h} \right) + \frac{\partial}{\partial y} \left(\frac{q_y^2}{h} + \frac{gh^2}{2} \right) = -gh \frac{\partial z_b}{\partial y} - \frac{\tau_{b,y}}{\rho} \quad (3)$$

64 where z_b is the bed elevation, h is the water depth, (q_x, q_y) are the two components
 65 of the unit discharge, $(\tau_{b,x}, \tau_{b,y})$ are the two horizontal components of the bed fric-
 66 tion stress, ρ is the water density and g is the gravity acceleration. Turbulent shear
 67 stresses have been neglected in Equations (2-3) because under runoff conditions,
 68 with water depths of a few millimetres, their influence in the momentum equations
 69 is negligible compared to bed friction.

70 The bed friction stress in Equations (2-3) can be expressed as:

$$\frac{\tau_{b,x}}{\rho} = C_f |\mathbf{U}| U_x \quad \frac{\tau_{b,y}}{\rho} = C_f |\mathbf{U}| U_y \quad (4)$$

71 where $|\mathbf{U}|$ is the modulus of the depth-averaged horizontal velocity, (U_x, U_y) are
72 the two horizontal components of the depth-averaged velocity, and C_f is a friction
73 coefficient. Several bed friction formulations have been considered in the simu-
74 lations presented in this paper, including the formulas of Keulegan, Manning and
75 Darcy for rough turbulent flow, the formula of Colebrook-White for smooth and
76 rough turbulent flow, and the formula for laminar flow (Table 1).

77 The shallow water equations are solved with a finite volume solver. The nu-
78 merical schemes used in the solver assure the conservation of mass, so that no wa-
79 ter is lost or gained during the computation due to numerical errors. The convec-
80 tive terms are discretized with an explicit high-order Godunov type scheme based
81 on Roe's approximate Riemman solver (LeVeque, 2002). Godunov schemes are
82 commonly used in shallow water codes because they can deal efficiently with the
83 development of shock waves, providing accurate and stable results (Toro, 2001).
84 This is especially interesting in rapidly varying flow applications, where regions
85 of subcritical and supercritical flows coexist, as it is the case of overland flow over
86 a complex topography. The bed elevation and bed friction terms in the momentum
87 equations are discretized with the upwind scheme presented in Cea and Vázquez-
88 Cendón (2012). A semi-implicit discretization scheme is used for the bed friction
89 to enhance the numerical stability of the solver. In order to model the wetting and
90 drying of certain regions of the spatial domain, the control volumes are allowed to
91 wet and dry during the simulation. For that purpose a wet-dry tolerance parameter
92 is defined, such that if the water depth in a cell is lower than this tolerance the cell
93 is considered to be dry. The water depth is never forced to be zero, in order to

94 keep the mass conservation property of the scheme. In all the simulations pre-
95 sented in this paper the wet-dry tolerance parameter was set to 0.01 mm. Model
96 output was insensitive to further reductions of this value. A detailed description
97 of the numerical schemes used in the solver can be found in Cea et al. (2010a) and
98 in Cea and Vázquez-Cendón (2012).

99 **3. EXPERIMENTAL TEST CASES AND DATASETS**

100 *3.1. Experimental test cases*

101 Two moulds of terrain with different complexity were used in the laboratory
102 experiments, which will be referred to as sinusoidal mould (Figure 1) and agricul-
103 tural mould (Figure 2a). The sinusoidal mould is a square of 1.20 m by 1.20 m
104 which consists of three parallel crests and furrows with a sinusoidal shape, with
105 a wave length of 0.20 m and an amplitude of 0.01 m. The DTM was measured
106 with a spatial resolution of 0.5 mm. The surface of the sinusoidal mould is made
107 of a thin layer of sand with a mean diameter of approximately 0.5-1.0 mm, which
108 is glued to an impervious surface. Therefore, there is no infiltration in the experi-
109 ments. We will refer by micro-roughness to the bed roughness linked to the sand
110 texture. The water supply was located on the upper part of the surface. The inlet
111 was 0.10 m wide and was set perpendicular to the direction of the largest slope
112 on each test case. Four different combinations of flow rates and slopes on the si-
113 nusoidal mould have been considered for model validation (Table 2). The slopes
114 in the X- and Y-directions as well as the input flow rates were selected experi-
115 mentally to obtain specific conditions that would help in assessing the quality of
116 the modelling results. In the different test cases water flows in 1, 2 or 3 furrows,
117 while always being at the limit of overflowing to the next one. For these experi-

118 mental conditions the water depth was less than 10 mm in the whole mould. The
119 Reynolds number in the main furrows varies between 1000 and 12000, depending
120 on the test case and on the furrow considered, while the Froude number varies
121 between zero and 5, although in most of the mould it is larger than one.

122 The agricultural mould is a square of 0.60 m by 0.60 m representative of a
123 seedbed. The mould is a perfect reproduction of a natural seedbed obtained with a
124 methodology similar to the one presented in Kamphorst and Duval (2001). All the
125 experiments were performed on that single reproduction. It exhibits two main par-
126 allel furrows oriented along the X-direction. The width of these furrows is of the
127 order of 0.10-0.15 m (Figure 2e). The surface of the agricultural mould is made of
128 plaster and is therefore much smoother than that of the sinusoidal mould. On the
129 other hand, in the agricultural mould there is a macro-roughness formed by small
130 changes in surface topography, as a result of different sized soil aggregates present
131 in the actual seedbed. In order to determine how the representation of these small
132 topographic changes is affected by the DTM resolution, we have filtered the orig-
133 inal DTM using average filters of different size, and we have defined the residual
134 length at each point of the mould as the difference between the original and filtered
135 DTM's. The spatial resolution of the original agricultural mould DTM is 2 mm.
136 A filter of 4 mm produces almost no effect on the original DTM, which confirms
137 that this resolution is high enough to capture all the topography features. A filter
138 of 8 mm gives an average residual length of 0.35 mm and a maximum residual
139 length of 6 mm, which is of the order of magnitude of the water depth. If the
140 filter size is increased to 16 mm the maximum residual length increases to 12 mm.
141 Larger filters introduce a smoothing effect in the macrotopography and distort the
142 definition of the two main longitudinal furrows (Figure 2c and d). The water was

143 supplied on the whole width of the upper part of the surface. However, the water
144 systematically enters the mould through the two main furrows, as indicated by the
145 arrows in Figure 2a. Two combinations of flow rates and slopes in the X-direction
146 on the agricultural mould have been used for model validation (Table 2). These
147 were selected in such a way that water flows either in two separated furrows or
148 in two connected furrows. In this case, only the velocity field was available for
149 model validation.

150 3.2. Datasets

151 For evaluation and comparison purposes, all measurements were performed at
152 steady state. The flow rates were measured separately at the outlet of each furrow
153 by automatically weighing the volume of water for 20 s to 2 min depending on the
154 flow rate for the sinusoidal mould. For the agricultural mould, the total flow rates
155 were measured by manual sample collection at the outlet every 2 min.

156 The maps of flow depth in the sinusoidal mould were obtained after subtraction
157 of two elevation maps acquired successively (i.e., subtraction of the water surface
158 map from the DTM without water). Both elevation datasets were measured using
159 the instantaneous profile laser scanner described in Darboux and Huang (2003)
160 according to the protocol presented in Legout et al. (2012). The spatial resolution
161 was 0.5 mm in X- and Y-directions. The uncertainty was experimentally assessed
162 to 0.5 mm with maximum values of 1 mm. It should be remarked that the maps of
163 flow depths were not measured on the agricultural mould.

164 The maps of surface velocity measurements were obtained by Large Scale Par-
165 ticle Image Velocimetry. Based on the acquisition of successive images of tracers
166 flowing on the surface, the LSPIV technique estimates the movement of tracer
167 particles between image pairs using a cross-correlation analysis. More details on

168 the adaptation of this well-known technique to the case of very shallow flows such
169 as overland flow are presented in Legout et al. (2012). The spatial resolution of
170 the velocity map was 5 mm. The ratios between surface velocities obtained with
171 LSPIV and the average velocity on the water column were estimated in Legout
172 et al. (2012) as 0.8 and 0.9 respectively on the sinusoidal and agricultural mould.
173 In the following section, the velocity measurements were corrected by those ratios
174 for the comparison between the experimental surface velocity and the modelled
175 depth-averaged velocity. The uncertainty of the surface velocities was experimen-
176 tally assessed to 0.03 m/s with maximum values of roughly 0.10 m/s.

177 **4. RESULTS AND DISCUSSION**

178 In this section we analyze the performance of the overland flow model pre-
179 sented in section 2 against the experimental data described in section 3. Model
180 performance is evaluated by comparing the spatial distribution of water depth
181 and velocity. In order to quantify the numerical-experimental agreement, the root
182 mean square error is computed for each simulation. As mentioned in section 3,
183 in the agricultural mould there are no available water depth measurements and
184 therefore, only the velocity field is used for comparison.

185 *4.1. Mesh convergence*

186 The mesh size is a critical parameter in any numerical model, as it has im-
187 portant consequences on the accuracy of the results, as well as on the compu-
188 tation time required to solve the model equations. Considering that the level of
189 macro-roughness of the two terrains considered in this study is very different, an
190 independent mesh convergence analysis was performed for each terrain, using for
191 that purpose the flow conditions of the test cases S1 (sinusoidal mould) and A1

192 (agricultural mould). Table 3 shows the properties of the different grids used in
193 the mesh convergence analysis.

194 The topography of the sinusoidal mould is quite smooth and regular and there-
195 fore, its main features are well captured even with a rather coarse mesh. On the
196 other hand the agricultural mould has a more irregular topography, including soil
197 aggregates up to 10-20 mm in size. In this case the mesh size has an important
198 impact on the accuracy of the bed elevation definition. The spatial resolution of
199 meshes A1M2, A1M3 and A1M4 (Table 3) is lower than that of the original DTM
200 and therefore, there is a loss of accuracy in the bed topography used in the numer-
201 ical model.

202 In both the sinusoidal and the agricultural terrains, the results obtained with
203 the two finest meshes (S1M1 and S1M2 in the sinusoidal mould and A1M1 and
204 A1M2 in the agricultural mould) are almost identical, and show similar flow pat-
205 terns to those obtained with meshes S1M3 and A1M3 respectively (Figures 3 and
206 4). Nonetheless, the maximum water depths and velocities are slightly diffused
207 with the latter meshes. The results obtained with the meshes S1M4 and A1M4
208 are clearly very diffusive and are not able to capture the maximum values of the
209 water depth and velocity, although the general flow pattern can still be identified.
210 Therefore, we have decided to work with the mesh S1M2 in the sinusoidal mould
211 and A1M2 in the agricultural mould, which have a spatial resolution of 5 mm
212 and 4 mm respectively. These meshes show a good compromise between com-
213 putation time and accuracy on model output (Table 3). Results obtained with the
214 finest meshes (S1M1 and A1M1) do not show significant differences while the
215 computation time increases considerably.

216 4.2. Keulegan formulation applied to the sinusoidal mould

217 The surface of the sinusoidal mould is made of sand grains with a diameter
218 within 0.5 and 1.0 mm. In non-cohesive beds without bedforms, river hydraulics
219 manuals recommend to use a roughness height within 1 and 3 times the diameter
220 of the sediment (Garcia, 2006). Based on this approximation, we have used a
221 roughness height of $k_s = 1.5$ mm in the simulations of the sinusoidal mould test
222 cases. It should be noticed that this approximation is recommended for river flows
223 and not specifically for overland flows, where the water depth in some regions
224 might be of the same order of magnitude as the roughness height. Nonetheless,
225 as it will be shown in the following this bed roughness coefficient gives very
226 satisfactory results in the four sinusoidal mould test cases.

227 Using Keulegan formulation with $k_s = 1.5$ mm the overall experimental-
228 numerical agreement is very satisfactory (Figures 5-11). The model predicts cor-
229 rectly the number of furrows which contribute to drain the inlet discharge (3 fur-
230 rows in test cases S1 and S2, two furrows in test case S3, and one single furrow
231 in test case S4). The prediction of the water depth field is very good in the four
232 test cases. The root mean square errors on the water depth are 0.6 mm, 0.7 mm,
233 0.7 mm and 0.9 mm for the test cases S1 to S4 respectively (Table 4), which are
234 of the same order of magnitude as the diameter of the sediment which covers the
235 mould surface. In all test cases the error on the water depth is less than 1 mm in
236 more than 90% of the measurement points, while it is greater than 2 mm in less
237 than 1% of the points (Figure 9). The accuracy on the prediction of the hydraulic
238 jump which appears in the test cases S1 and S4 at the location $y = 0.78$ m in the
239 profile $x = 0.8$ m is remarkable (Figure 11).

240 The comparison of the measured and computed velocities has a larger un-

241 certainty for two reasons. Firstly, the LSPIV technique gives abnormally small
242 velocities in regions where the water depth is very small, because the tracers oc-
243 casionally rest attached to the rough bed surface. This occurs typically at the flow
244 inlet and in the crests between furrows. In order to compare the velocities only
245 the points in which the unit discharge is larger than $0.5 \text{ cm}^2/\text{s}$ were considered.
246 This value was adopted because it defines rather precisely the shape of the furrows
247 (Figures 5-8), and it excludes the regions where the LSPIV velocity has large mea-
248 surement errors. Another source of uncertainty in the comparison of velocity data
249 is the fact that LSPIV measures the surface velocity, while the numerical model
250 computes the depth-averaged velocity. In order to estimate the surface velocity
251 from the model output, the ratios mentioned in Legout et al. (2012) and in sec-
252 tion 3.2 were adopted. With these criteria, the root mean square errors on the
253 velocity are 0.089 m/s, 0.058 m/s, 0.083 m/s and 0.065 m/s respectively for the
254 test cases S1 to S4 (Figure 10).

255 It should be noted that in the test case S1 (Figure 5), there is a clear disagree-
256 ment between numerical predictions and experimental data in the third furrow,
257 which is the one with the smallest water depth. The experimental measurements
258 of water depth and velocity reveal a region between $x = 0.1 \text{ m}$ and $x = 0.4 \text{ m}$
259 where the flow is locally accelerated (higher velocity and lower water depth). The
260 same effect appears in the test case S3 (Figure 7), but in this case in the second
261 furrow (which is in this case the one which presents the smallest water depths).
262 This local acceleration does not appear in the numerical model, as it can be ob-
263 served in the velocity fields shown in Figures 5 and 8, and it is the reason why
264 the root mean square error is larger in these test cases than in the cases S2 and
265 S4. This discrepancy is represented in Figure 10 by the cloud of points in which

266 the LSPIV velocity is clearly higher than the numerical velocity. We have tried
267 unsuccessfully to improve the velocity predictions in these regions using different
268 bed friction formulations (see section 4.3). We have not found a clear physical
269 explanation for this effect.

270 *4.3. Other bed friction formulations applied to the sinusoidal mould*

271 The results shown in the previous section indicate that Keulegan formulation
272 with a definition of the roughness height based on the physical properties of the
273 mould surface (in our case the sediment diameter) performs satisfactorily in the
274 sinusoidal mould. As roughness formulations are known to affect significantly the
275 model performance (Mügler et al., 2011), we have explored the possibility of im-
276 proving the predictions of the model by using other bed friction parameterizations.
277 For that purpose we have considered the standard bed friction formulations shown
278 in Table 1. Three of these formulations (Keulegan, Manning and Darcy with a con-
279 stant friction factor) were developed for rough turbulent flow. The forth formu-
280 lation is based on the formula of Colebrook-White, and considers the transitions
281 between laminar flow, smooth turbulent flow and rough turbulent flow. In this
282 latter formulation the laminar bed friction formula is used if the local Reynolds
283 number is smaller than 2000 ($4Uh/\nu < 2000$), otherwise the Colebrook-White
284 equation is applied. In all cases the bed roughness parameter was calibrated for
285 the test case S1 and then used in the test cases S2, S3 and S4.

286 After calibration of their respective friction parameters, all the parameteri-
287 zations give a similar agreement with the experimental data (Tables 4 and 4).
288 Their performance considering the water depth and velocity spatial distributions
289 is rather satisfactory, specially regarding the water depth. The agreement in the
290 velocity field is slightly better when using Keulegan or Manning formulations,

291 although the performance of Darcy and Colebrook-White formulations is still ac-
292 ceptable. The main advantage of Keulegan parameterization is that the roughness
293 height is more easily related to the roughness characteristics of the terrain than the
294 Manning or Darcy coefficients.

295 4.4. Agricultural mould

296 The most significant difference between the sinusoidal and the agricultural
297 moulds is that the latter one includes soil aggregates which create a certain level
298 of macro-roughness. As shown in Figure 2, the size and location of the soil ag-
299 gregates is well captured by the numerical meshes with a spatial resolution of
300 2 mm and 4 mm (A1M1 and A1M2), but they are reduced as the grid resolution is
301 reduced. The macro-roughness generated by these soil aggregates induces small
302 scale accelerations and decelerations in the flow field, causing additional head
303 losses. One of the purposes of the agricultural terrain test cases is to analyze if a
304 high resolution shallow water model with a micro-roughness coefficient defined
305 from the bed material (in this case plaster) is able to reproduce the experimental
306 velocity field.

307 Test case A1 has been used for model calibration and to analyze how the
308 bed friction coefficient should be modified in order to account for the macro-
309 roughness. Test case A2 has been used for model validation, using the same
310 roughness parameterization as in case A1.

311 Figure 12 shows that the velocity field computed using a bed roughness coeffi-
312 cient for plaster (either $k_s = 1$ mm in Keulegan formulation or $n = 0.013$ s m^{-1/3}
313 in Manning formulation) are far from the experimental ones, even if the com-
314 putations were done with a high resolution mesh which includes all the small
315 scale details of the topography. The computed velocities are too large compared

316 with the LSPIV measurements. The root mean square error obtained with Keule-
317 gan and Manning formulas using these parameters are respectively 0.095 m/s and
318 0.100 m/s (Table 5).

319 Model outputs is improved significantly if a larger bed friction coefficient
320 is used. After calibration, the coefficients which produce the best numerical-
321 experimental agreement were found to be $k_s = 30$ mm and $n = 0.050$ s m^{-1/3},
322 the root mean square error for the velocity being 0.040 m/s for both cases. The
323 velocity fields computed with these parameters show a good global agreement
324 with the LSPIV data (Figure 12). Both, experimental and numerical results show
325 a shallow and narrow arm which develops to the left of the upper furrow and joins
326 the lower furrow further downstream.

327 It can be noticed in Figure 12 that the numerical model gives some locally
328 high velocity values which do not appear in the experimental data. These local
329 velocity peaks are due to the highly irregular topography created by the soil ag-
330 gregates. The energy losses induced by these high frequency accelerations are
331 not well represented by the shallow water equations with the standard bed friction
332 formulations, even if a very detailed grid and DTM are used in the computations.
333 This explains the high value of the bed friction coefficient found in the calibration
334 ($k_s = 30$ mm and $n = 0.050$ s m^{-1/3}).

335 The roughness coefficient in Keulegan formulation might be related to the
336 macro-roughness of the bed surface. For this purpose, the roughness height in
337 Keulegan formulation was defined on a physical basis as $k_s = Al_\Delta$, where l_Δ is
338 a local measure of the macro-roughness length scale, and A is a constant of order
339 1. The level of macro-roughness in the agricultural mould is not homogeneous,
340 the spatial density and size of the soil aggregates in the upper furrow being lower

341 than in the lower furrow. Therefore, a spatially variable macro-roughness length
342 scale l_{Δ} was defined from the residuals (Δz) obtained after filtering the original
343 DTM with an average filter of size Δ . After trying several definitions of l_{Δ} and
344 filter sizes, a suitable definition for the roughness height was obtained with $A = 1$,
345 and $l_{\Delta} = \max(\Delta z)$, where the residuals Δz are computed using an average filter
346 of size $\Delta = 10$ mm. The velocity results obtained using this *macro-roughness*
347 *based* definition for the roughness height ($k_s = \max(\Delta z)$) are shown in Fig-
348 ure 12. There is not a significant improvement relative to the results obtained with
349 a constant roughness coefficient ($k_s = 30$ mm), but in this case the values of k_s
350 vary locally according to the physical characteristics of the macro-roughness, as
351 shown in Figure 13.

352 The same roughness parameterizations applied to the test case A2 gives sat-
353 isfactory results (Figure 13). Although the quantitative agreement between nu-
354 merical and experimental data is not as good as in test case A1 (Table 5), the
355 differences are of the same order as the uncertainty on the experimental surface
356 velocity (section 3.2). This increase in the root mean square error is to some extent
357 explained by the gaps in the experimental velocity data which can be observed in
358 Figure 13. Due to the extremely low water depths and the high surface roughness
359 of the agricultural mould, there are some isolated spots in which tracers could not
360 move and thus velocity was not correctly measured. This introduces spurious dis-
361 agreements with the numerical model which are reflected in the root mean square
362 error. Nonetheless, visual comparison of the velocity fields in Figure 13 shows a
363 similar global agreement to that of test case A1.

364 5. CONCLUSIONS

365 The performance of an overland flow model based on the two-dimensional
366 shallow water equations has been analyzed using high-resolution distributed mea-
367 surements of water depth and velocity. Several flow conditions over two impervi-
368 ous moulds with different micro and macro-roughness characteristics have been
369 used for model validation.

370 The flow in the sinusoidal mould, which represents a terrain with a regular to-
371 pography and no macro-roughness, is properly represented by the two-dimensional
372 shallow water equations with a constant bed friction coefficient. This latter can
373 be related to the micro-roughness characteristics of the bed surface. Manning and
374 Keulegan formulations produce results with similar accuracy. More complex for-
375 mulations which consider the transitions between laminar, smooth turbulent and
376 rough turbulent flow conditions, do not improve model performance.

377 In terrains with a certain level of macro-roughness, as it is the case of the agri-
378 cultural mould with soil aggregates, the two-dimensional shallow water equations
379 with a bed friction coefficient defined from the micro-roughness of the bed sur-
380 face are not able to accurately reproduce the flow field. This is because the soil
381 aggregates which define the macro-roughness produce small scale accelerations
382 and decelerations in the flow field, which generate additional head losses. Even
383 if the mesh size is smaller than the soil aggregates, these head losses cannot be
384 captured by the model equations. In order to correctly reproduce the flow hydro-
385 dynamic, the bed roughness coefficient must account for the macro-roughness of
386 the terrain generated by the presence of soil aggregates.

387 In the agricultural mould the bed roughness height used in Keulegan formu-
388 lation (k_s) could be related to the local macro-roughness length scale of the bed

389 surface (l_{Δ}) by the simple relation ($k_s = l_{\Delta}$). In the test cases analyzed in this
390 work a proper definition of l_{Δ} is the maximum residual obtained after filtering the
391 original DTM with a filter size of 10 mm, and it is related to the size of the soil
392 aggregates. The problem with this approach when applied to larger scales is that
393 a very fine spatial resolution is required in order to apply a 10 mm filter to the
394 DTM, which limits the applicability of a *macro-roughness based* definition of k_s .

395 These results show that using a physically-based definition of the bed rough-
396 ness coefficient, a two-dimensional shallow water model is able to reproduce the
397 velocity and water depth patterns under runoff conditions. In the test cases ana-
398 lyzed in this paper the average errors on the water depth and velocity were 0.7 mm
399 and 0.07 m/s respectively. This justifies the use of the shallow water equations in
400 physically-based erosion and solute transport models that require a very detailed
401 spatial characterization of the flow field in order to take advantage of their full
402 potential. Regarding the applicability of the model to larger scales, and thus more
403 relevant for hillslope hydrology understanding, the limiting factor is the DEM and
404 mesh resolution required for the computations. A spatial resolution of the order of
405 10 mm is required to capture the flow patterns and the range of depth and velocity
406 values. Applying such a high resolution shallow water model to plot scales of a
407 few hundreds of square meters would lead to reasonable computation times (of
408 the order of 5 h in a standard laptop for a 100 m² plot). Such resolution is also
409 consistent with what can be obtained from stereophotogrammetry or laser scanner
410 techniques in field conditions.

411 **References**

- 412 Abrahams, A.D., Li, G., Krishnan, C., Atkinson, J.F., 1998. Predicting sediment
413 transport by interrill overland flow on rough surfaces. *Earth Surf. Process. Land-*
414 *forms* 23, 1087–1099.
- 415 Cea, L., Garrido, M., Puertas, J., 2010a. Experimental validation of two-
416 dimensional depth-averaged models for forecasting rainfall-runoff from pre-
417 cipitation data in urban areas. *Journal of Hydrology* 382, 88–102.
- 418 Cea, L., Garrido, M., Puertas, J., Jácome, A., del Río, H., Suárez, J., 2010b. Over-
419 land flow computations in urban and industrial catchments from direct precip-
420 itation data using a two-dimensional shallow water model. *Water Science and*
421 *Technology* 62, 1998–2008.
- 422 Cea, L., Vázquez-Cendón, M.E., 2012. Unstructured finite volume discretiza-
423 tion of bed friction and convective flux in solute transport models linked to the
424 shallow water equations. *Journal of Computational Physics* 231, 3317–3339.
- 425 Fraga, I., Cea, L., Puertas, J., 2013. Experimental study of the water depth and
426 rainfall intensity effects on the bed roughness coefficient used in distributed
427 urban drainage models. *Journal of Hydrology* 505, 266–275.
- 428 Darboux, F., Huang, C., 2003. An instantaneous-profile laser scanner to measure
429 soil surface microtopography. *Soil Sci. Soc. Am. J.* 67, 92–99.
- 430 Garcia, M.H., 2006. *Sedimentation Engineering: Processes, Measurements, Mod-*
431 *eling, and Practice*. ASCE, Reston, Virginia.

- 432 Hairsine, P.B., Rose, C.W., 1992a. Modeling water erosion due to overland-flow
433 using physical principles. 1. rill flow. *Water Resources Research* 28, 245–250.
- 434 Hairsine, P.B., Rose, C.W., 1992b. Modeling water erosion due to overland-flow
435 using physical principles. 1. sheet flow. *Water Resources Research* 28, 237–
436 243.
- 437 Howes, D.A., Abrahams, A.D., Pitman, E.B., 2006. One- and two-dimensional
438 modelling of overland flow in semiarid shrubland, jornada basin, new mexico.
439 *Hydrol. Process.* 20, 1027–1046.
- 440 Jarvela, J., 2002. Flow resistance of flexible and stiff vegetation: a flume study
441 with natural plants. *Journal of Hydrology* 269, 44–54.
- 442 Jomaa, S., Barry, D.A., Brovelli, A., Sander, G.C., Parlange, J.Y., Heng,
443 B.C.P., van Meerveld, H.J.T., 2010. Effect of raindrop splash and transversal
444 width on soil erosion: Laboratory flume experiments and analysis with the
445 Hairsine–Rose model. *Journal of Hydrology* 395, 117–132.
- 446 Kamphorst, E.C., Duval, Y., 2001. Validation of a numerical method to quantify
447 depression storage by direct measurements on moulded surfaces. *CATENA* 43,
448 1–14.
- 449 Kivva, S.L., Zheleznyak, M.J., 2005. Two-dimensional modeling of rainfall runoff
450 and sediment transport in small catchments areas. *International Journal of Fluid
451 Mechanics Research* 32, 703–716.
- 452 Lawrence, D.S.L., 2000. Hydraulic resistance in overland flow during partial and
453 marginal surface inundation: Experimental observations and modeling. *Water
454 Resources Research* 36, 2381–2393.

- 455 Legout, C., Darboux, F., Nedelec, Y., Hauet, A., Esteves, M., Renaux, B., Denis,
456 H., Cordier, S., 2012. High spatial resolution mapping of surface velocities and
457 depths for shallow overland flow. *Earth Surface Processes and Landforms* 37,
458 984–993.
- 459 LeVeque, R.J., 2002. *Finite Volume Methods for Hyperbolic Problems*. volume 31
460 of *Cambridge Texts in Applied Mathematics*. Cambridge University Press.
- 461 Mügler, C., Planchon, O., Patin, J., Weill, S., Silvera, N., Richard, P., Mouche, E.,
462 2011. Comparison of roughness models to simulate overland flow and tracer
463 transport experiments under simulated rainfall at plot scale. *Journal of Hydrology*
464 402, 25–40.
- 465 Morgali, J.R., Linsley, R.K., 1965. Computer analysis of overland flow. *Journal*
466 of the Hydraulics Division. *Proceedings of the American Society of Civil*
467 *Engineers* HY3, 81–100.
- 468 Nord, G., Esteves, M., 2007. Evaluation of sediment transport formulae and de-
469 tachment parameters in eroding rills using PSEM2D and the Water Erosion
470 Prediction Project (WEPP) database. *Water Resources Research* 43, 1–14.
- 471 Nord, G., Esteves, M., 2010. The effect of soil type, meteorological forcing and
472 slope gradient on the simulation of internal erosion processes at the local scale.
473 *Hydrological Processes* 24, 1766–1780.
- 474 Shaw, S.B., Parlange, J.Y., Lebowitz, M., Walter, M.T., 2009. Accounting for
475 surface roughness in a physically-based urban wash-off model. *Journal of Hy-*
476 *drology* 367, 79–85.

Table 1: Bed friction formulations considered in the numerical simulations. f : Darcy's friction factor; k_s : roughness height; n : Manning coefficient; ν : kinematic viscosity of water (10^{-6} m²/s).

Formulation	Friction factor parameterization
Darcy (f)	$C_f = \frac{f}{8}$
Keulegan (k_s)	$C_f = 0.16 (\ln 11h/k_s)^{-2}$
Manning (n)	$C_f = g \frac{n^2}{h^{1/3}}$
Colebrook-White (k_s)	$C_f = 0.16 \left(-\ln \left(\frac{k_s}{11h} + \frac{2.5\nu}{11.9Uh\sqrt{C_f}} \right) \right)^{-2}$
Laminar	$C_f = \frac{3\nu}{ \mathbf{U} h}$

- 477 Shaw, S.B., Walter, M.T., Steenhuis, T.S., 2006. A physical model of particulate
478 wash-off from rough impervious surfaces. *Journal of Hydrology* 327, 618–626.
- 479 Tatard, L., Planchon, O., Wainwright, J., Nord, G., Favis-Mortlock, D., Silvera,
480 N., Ribolzi, O., Esteves, M., Huang, C.H., 2008. Measurement and modelling
481 of high-resolution flow-velocity data under simulated rainfall on a low-slope
482 sandy soil. *Journal of Hydrology* 348, 1 – 12.
- 483 Toro, E.F., 2001. *Shock-capturing Methods for Free-Surface Shallow Flows*. Wi-
484 ley, Chichester, West Sussex PO19 1UD, England.
- 485 Yan, M., Kahawita, R., 1989. Simulating the evolution of non-point source pollu-
486 tants in a shallow water environment. *Chemosphere* 67, 879–885.
- 487 Zhang, Cundy, 1989. Modeling of two-dimensional overland flow. *Water Re-
488 sources Research* 25, 2019–2035.

Table 2: Summary of experimental test cases used for model validation.

Test case	Mould	Surface	Flow rate (cm ³ /s)	Slope Y-dir (%)	Slope X-dir (%)
S1	sinusoidal	Sand	110	20.4	3.2
S2	sinusoidal	Sand	131	18.1	0.0
S3	sinusoidal	Sand	79	18.0	3.1
S4	sinusoidal	Sand	93	14.4	11.4
A1	agricultural	Plaster	182	0.0	4.0
A2	agricultural	Plaster	177	0.0	7.7

Table 3: Mesh convergence analysis for the sinusoidal and agricultural moulds. The results obtained with meshes S1M1 and A1M1 are used as a reference to compute the root mean square error in water depth (σ_h) and velocity (σ_v) on the coarser meshes. Δx is the mesh size, N_{nod} is the number of elements in the mesh, and T_c is the computation time with an Intel Core i7 - 1.60 GHz.

Test case	Mesh	Δx	N_{nod}	T_c	σ_h	σ_v
S1	S1M1	2 mm	170817	5400 s	-	-
S1	S1M2	5 mm	38971	340 s	0.17 mm	0.018 m/s
S1	S1M3	10 mm	9748	35 s	0.28 mm	0.034 m/s
S1	S1M4	20 mm	2467	4 s	0.67 mm	0.065 m/s
A1	A1M1	2 mm	115840	4200 s	-	-
A1	A1M2	4 mm	28960	600 s	-	0.013 m/s
A1	A1M3	8 mm	6400	60 s	-	0.031 m/s
A1	A1M4	16 mm	1600	8 s	-	0.265 m/s

Table 4: Performance of different bed friction parameterizations in the test cases S1, S2, S3 and S4, evaluated as the root mean square error of the water depth (σ_h) and velocity (σ_v).

Parameterization	σ_h (mm)				σ_v (m/s)			
	S1	S2	S3	S4	S1	S2	S3	S4
Keulegan ($k_s = 1.5$ mm)	0.6	0.7	0.7	0.9	0.089	0.058	0.083	0.065
Manning ($n = 0.015$ s m ^{-1/3})	0.6	0.7	0.6	0.9	0.094	0.070	0.084	0.068
Darcy ($f = 0.16$)	0.6	0.8	0.8	1.1	0.099	0.063	0.088	0.100
Colebrook-White ($k_s = 1.5$ mm)	0.8	0.7	0.6	1.0	0.098	0.067	0.090	0.110

Table 5: Performance of different bed friction parameterizations in the test cases A1 and A2 in the agricultural mould, evaluated as the root mean square error of the velocity.

Parameterization	Friction factor	A1	A2
Keulegan	$k_s = 1$ mm	0.095 m/s	0.140 m/s
Keulegan	$k_s = 30$ mm	0.040 m/s	0.062 m/s
Manning	$n = 0.013$ s m ^{-1/3}	0.100 m/s	0.150 m/s
Manning	$n = 0.050$ s m ^{-1/3}	0.040 m/s	0.071 m/s
Keulegan	$k_s = \max \Delta_z$	0.039 m/s	0.062 m/s

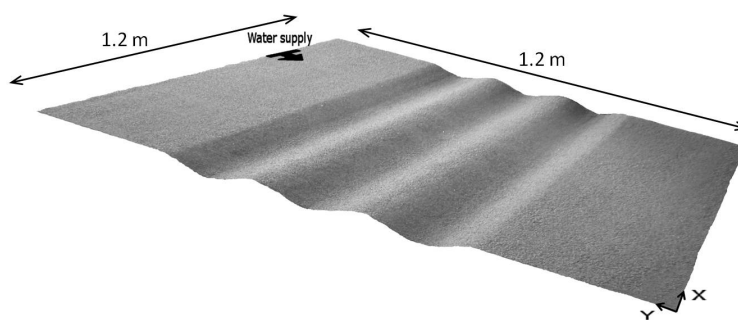


Figure 1: Representation of the sinusoidal mould.

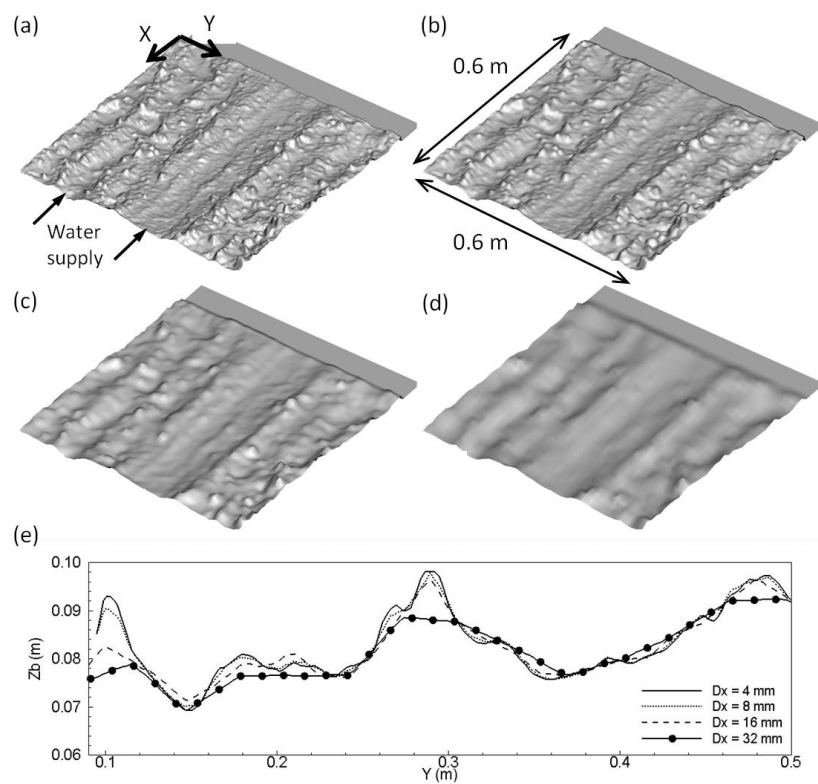


Figure 2: Representation of the agricultural seedbed mould after filtering the original DTM with several filter sizes (Δ). (a) Original DTM, (b) $\Delta = 4$ mm, (c) $\Delta = 8$ mm (d) $\Delta = 16$ mm , and (e) cross section at $x = 0.3$ m computed from the filtered DTM's.

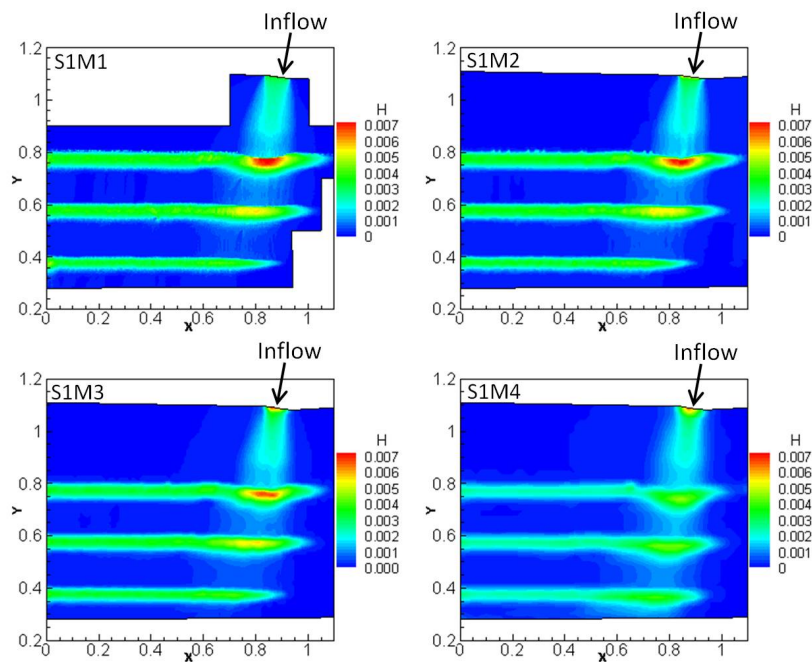


Figure 3: Mesh convergence in the sinusoidal mould. Water depth (m) computed with the meshes S1M1 (top-left), S1M2 (top-right), S1M3 (bottom-left) and S1M4 (bottom-right). Axes units in meters.

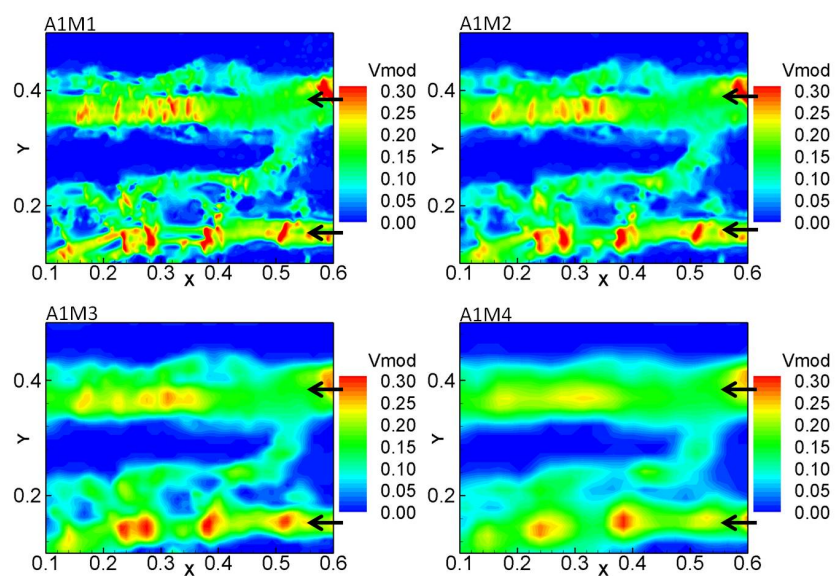


Figure 4: Mesh convergence in the agricultural mould. Black arrows indicate inflow locations. Velocity (m/s) computed with the meshes A1M1 (top-left), A1M2 (top-right), A1M3 (bottom-left) and A1M4 (bottom-right). Axes units in meters.

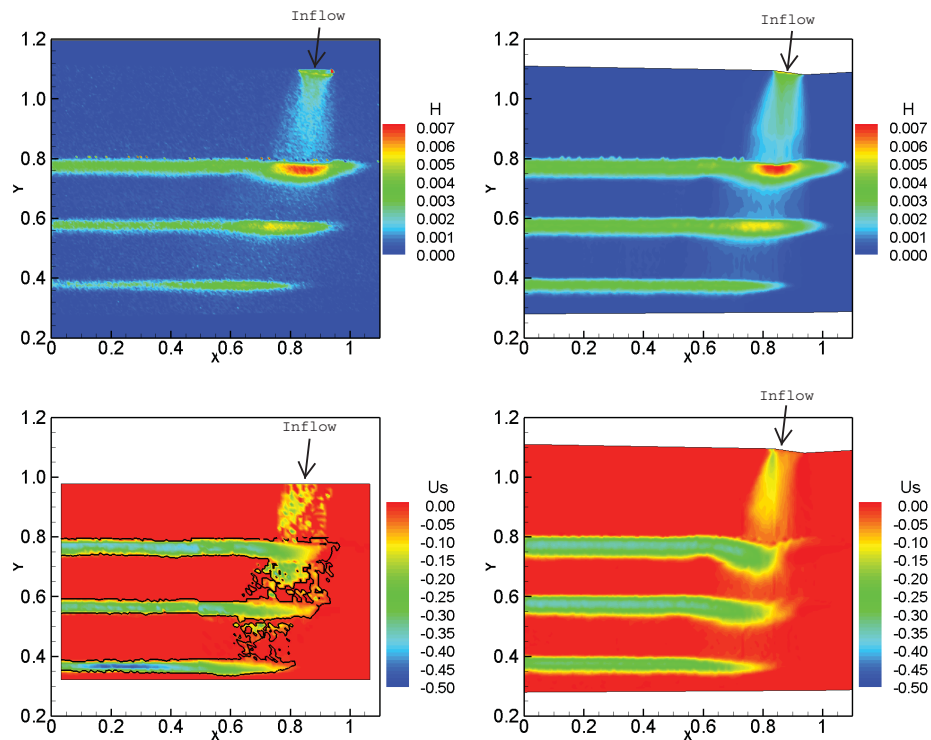


Figure 5: Experimental (left) and numerical (right) water depth (m) and surface velocity (m/s) fields for the test case S1. Numerical results were obtained with Keulegan formulation and $k_s = 1.5$ mm. The black contour defines the region used to compute the root mean square error for the velocity (Table 4). Axes units in meters.

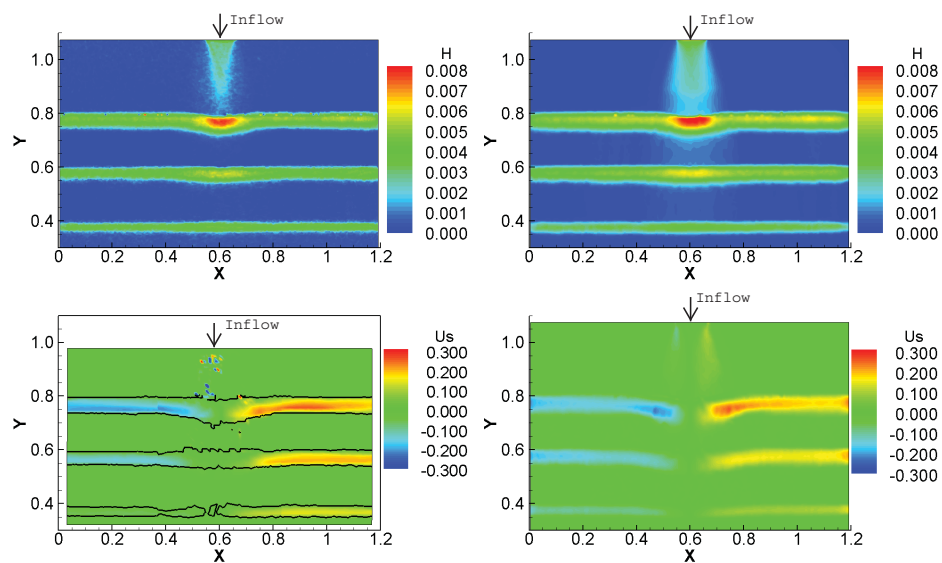


Figure 6: Experimental (left) and numerical (right) water depth (m) and surface velocity (m/s) fields for the test case S2. Numerical results were obtained with Keulegan formulation and $k_s = 1.5$ mm. The black contour defines the region used to compute the root mean square error for the velocity (Table 4). Axes units in meters.

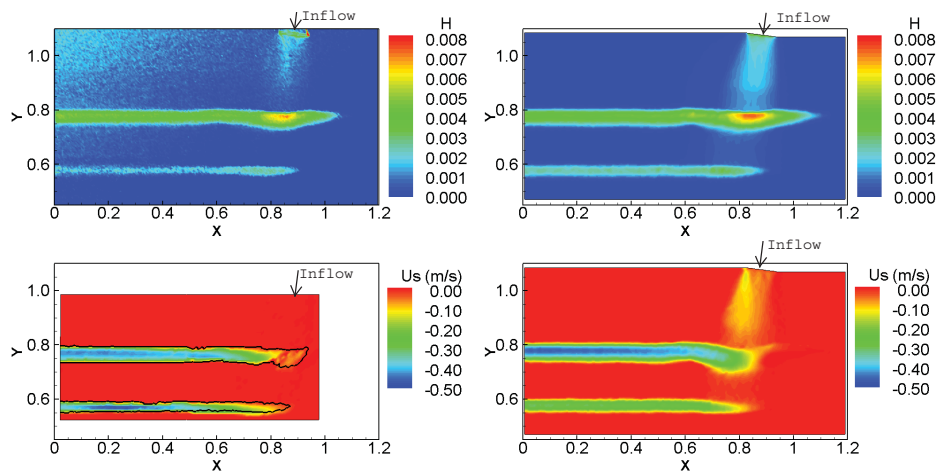


Figure 7: Experimental (left) and numerical (right) water depth (m) and surface velocity (m/s) fields for the test case S3. Numerical results were obtained with Keulegan formulation and $k_s = 1.5$ mm. The black contour defines the region used to compute the root mean square error for the velocity (Table 4). Axes units in meters.

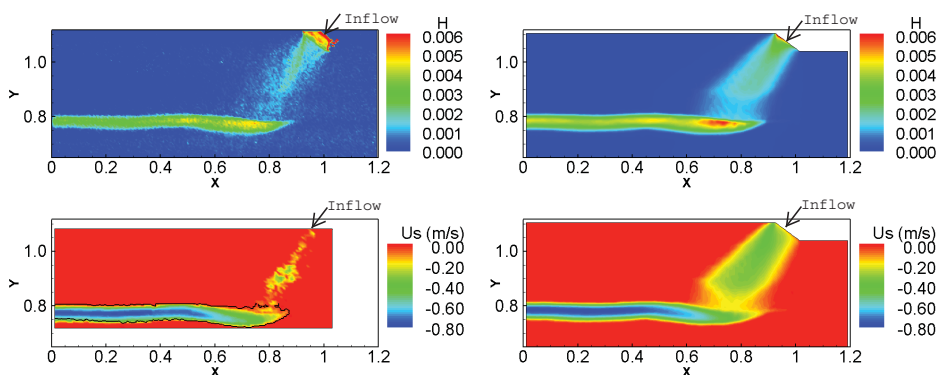


Figure 8: Experimental (left) and numerical (right) water depth (m) and surface velocity (m/s) fields for the test case S4. Numerical results were obtained with Keulegan formulation and $k_s = 1.5$ mm. The black contour defines the region used to compute the root mean square error for the velocity (Table 4). Axes units in meters.

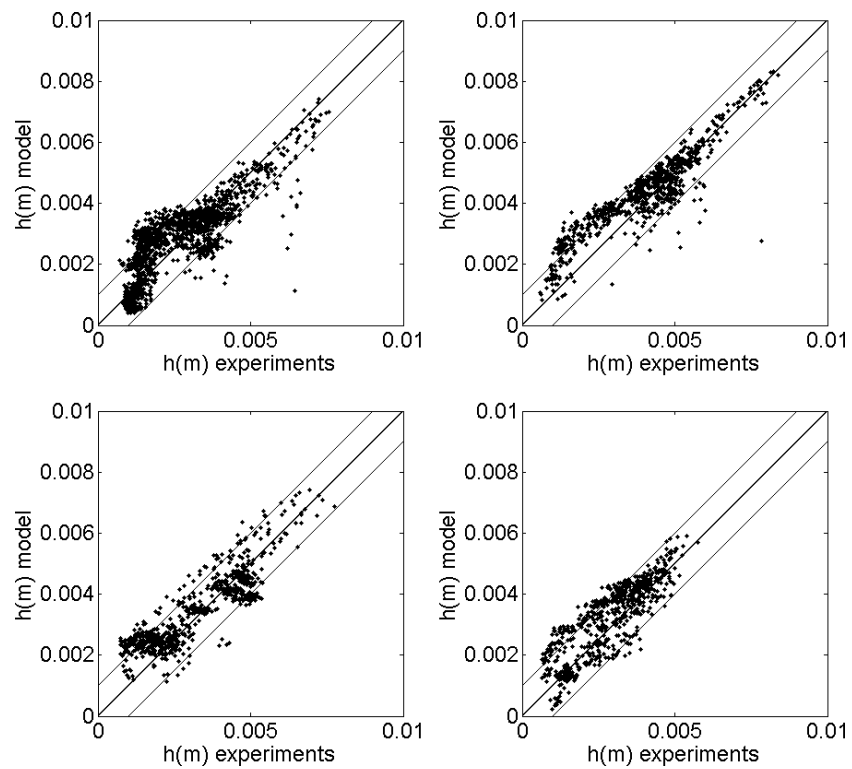


Figure 9: Computed vs. modelled water depths in the sinusoidal mould. Test cases S1 (top-left), S2 (top-right), S3 (bottom-left) and S4 (bottom-right). Lines above and below the 1:1 line correspond to the maximum experimental uncertainty of 1 mm.

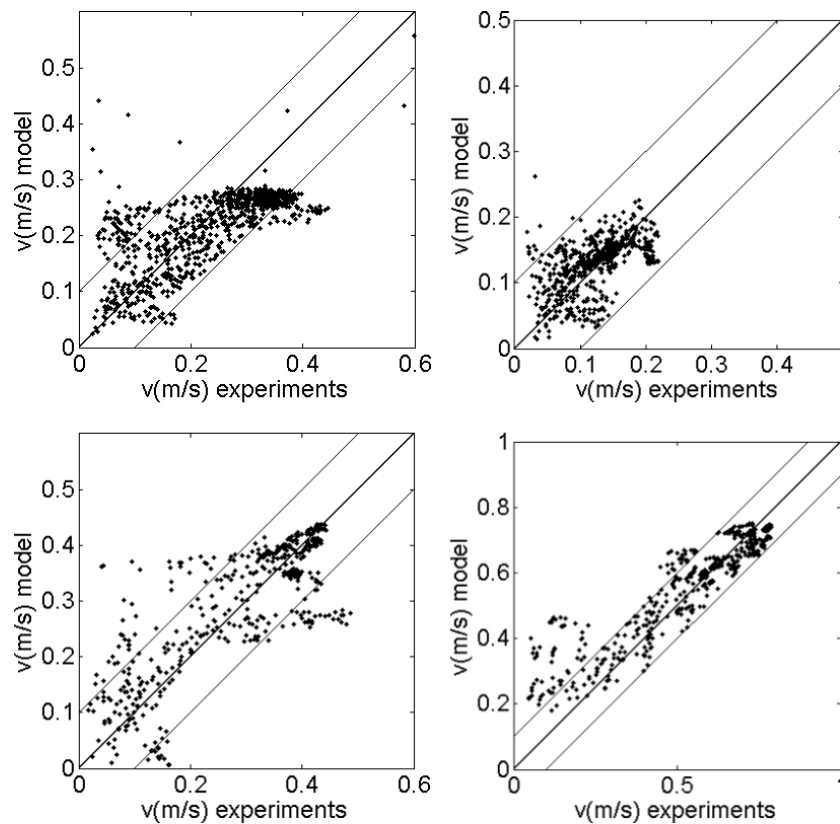


Figure 10: Computed vs. modelled velocities in the sinusoidal mould. Test cases S1 (top-left), S2 (top-right), S3 (bottom-left) and S4 (bottom-right). Lines above and below the 1:1 line correspond to the maximum experimental uncertainty of 0.10 m/s.

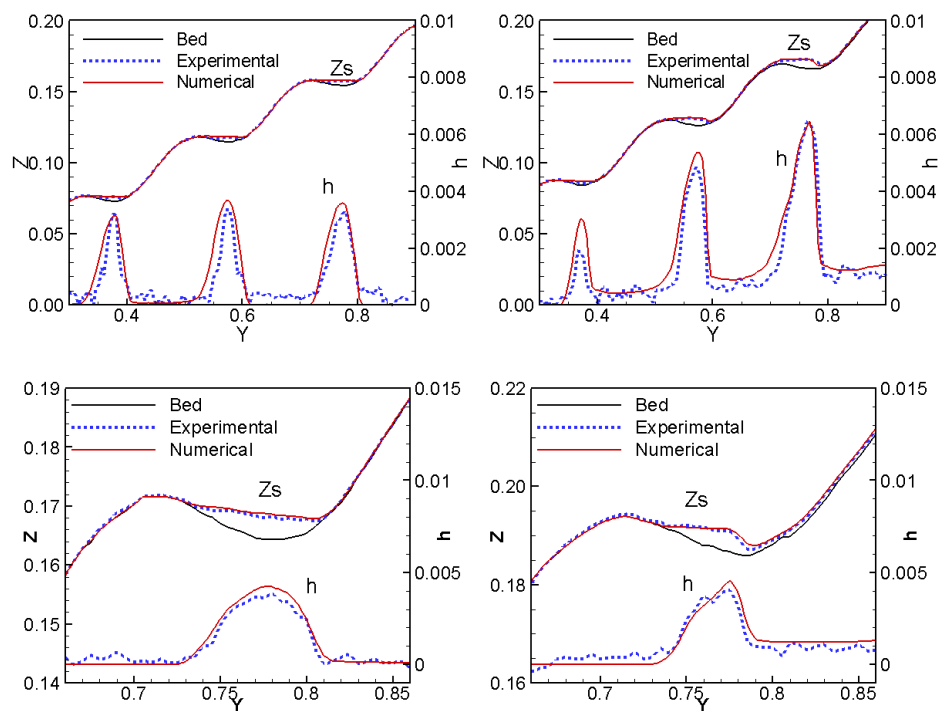


Figure 11: Experimental vs. numerical water depth (m) profiles in the sinusoidal mould. Test cases: S1 at $x = 0.4$ m (top-left), S1 at $x = 0.8$ m (top-right), S4 at $x = 0.6$ m (bottom-left) and S4 at $x = 0.8$ m (bottom-right).

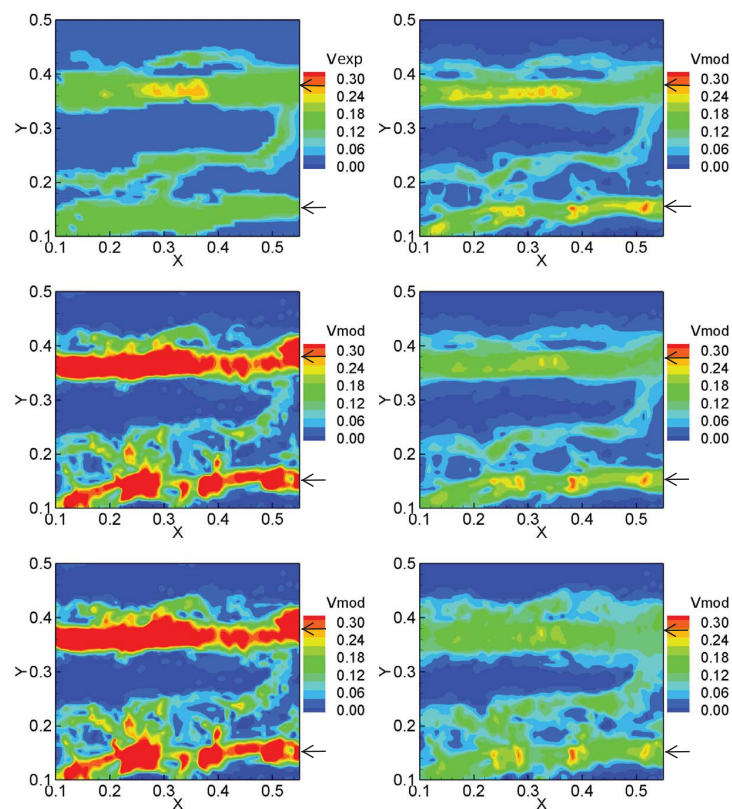


Figure 12: Velocity field (m/s) in the agricultural mould in the test case A1 using different bed roughness parameterizations. Black arrows indicate inflow locations. Experimental velocity (top-left) vs. numerical velocity computed with $k_s = \max \Delta z$ (top-right), $k_s = 1 \text{ mm}$ (middle-left), $k_s = 30 \text{ mm}$ (middle-right), $n = 0.013 \text{ s m}^{-1/3}$ (bottom-left) and $n = 0.050 \text{ s m}^{-1/3}$ (bottom-right).

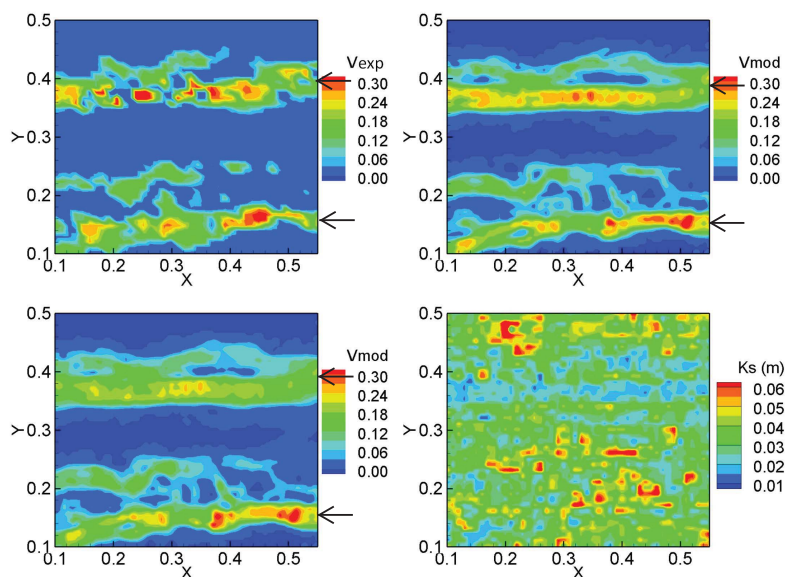


Figure 13: Velocity (m/s) field in the agricultural mould in the test case A2 using different bed roughness parameterizations. Black arrows indicate inflow locations. Experimental velocity (top-left) vs. numerical velocity computed with $k_s = \max \Delta_z$ (top-right) and $k_s = 30$ mm (bottom-left). The bottom-right figure shows the spatial distribution of the roughness height computed from $k_s = \max \Delta_z$.